ENGINEERING Agriculture

Engineering Journals

RESEARCH ARTICLE

2027 / Volume 14 / Issue 2 / 27725

Remediation of phenanthrene-contaminated soil using a Schwertmannite activated persulfate system

Yanyan WANG (✉)[1], Weiqian WANG[2], Qingyue WANG (✉)[2]

1 College of Resources and Environment, Shanxi Agricultural University; Soil Health Laboratory in Shanxi Province, Taiyuan 030031, China.

2 Graduate School of Science and Engineering, Saitama University, 255 Shimo-Okubo, Sakura-ku, Saitama City 338-8570, Japan.

KEYWORDS

Schwertmannite, persulfate activation, phenanthrene, soil remediation, PAH degradation

HIGHLIGHTS

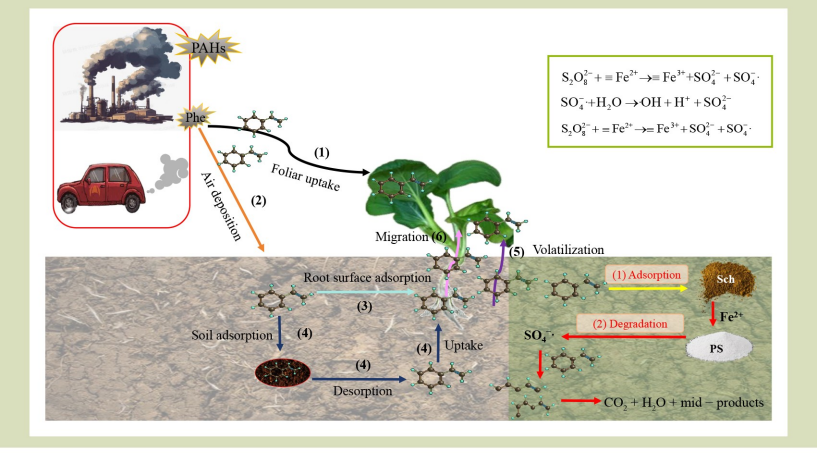
- Schwertmannite (Sch) + persulfate (PS) system can remove phenanthrene (Phe) from soil.
- Sch + PS system significantly promoted Bok choy growth performance.
- Sch combined with PS effectively suppresses Phe uptake and accumulation by Bok choy.

Received October 17, 2025;
Accepted May 11, 2026.

Correspondences: sxauwyy0811@163.com, seiyo@mail.saitama-u.ac.jp

Special Section: Towards Carbon Neutrality: Advances in Agricultural Production and Emission Reduction (Guest Editor: Hong Yang)

GRAPHICAL ABSTRACT



ABSTRACT

Polycyclic aromatic hydrocarbons, such as phenanthrene, have become widespread environmental contaminants due to industrial and incomplete combustion, posing serious risks to soil ecosystems and agricultural safety. This study conducted a pot experiment with seven treatments to investigate the remediation performance and ecological effects of a Schwertmannite-activated persulfate system on phenanthrene-contaminated soil. The concentrations of phenanthrene, persulfate, and Schwertmannite were 20 mg·kg^{-1}, 200 mg·kg^{-1}, and 1 g·kg^{-1}, respectively. The results revealed that the combined Schwertmannite-persulfate treatment was superior for soil remediation and *Brassica rapa* subsp. *Chinensis* protection. By leveraging the adsorption capability of Schwertmannite and its catalytic activation of persulfate to generate sulfate radicals (SO_4^{-}·), the system achieved 86.2% phenanthrene removal within 5 days, with the ultimate removal efficiency reaching 94.5%. Regarding plant development, the combined treatment improved *B. rapa* subsp. *Chinensis* growth, achieving a total biomass of 6.91 g per pot, and also inhibited Phe accumulation in plant tissues, reducing

phenanthrene concentrations in leaves, stems, and roots to 0.2, 0.2, and 0.3 mg·kg^{-1}, respectively. Taken together, this study demonstrates that the Schwertmannite-persulfate system was effective and environmentally compatible for remediating phenanthrene-contaminated soil, providing valuable insights for developing field-scale remediation strategies for PAH-contaminated soils.

© The Author(s) 2027. Published by Higher Education Press. This is an open access article under the CC BY license (http://creativecommons.org/licenses/by/4.0)

1 Introduction

As a fundamental resource for agricultural production and ecosystem integrity, soil is under increasing pressure from contamination with polycyclic aromatic hydrocarbons (PAHs). These persistent pollutants originate primarily from incomplete combustion of fossil fuel, industrial emissions, and accidental petroleum releases[1–3]. Regional investigations (such as those conducted in the Songnen Plain of China) have detected PAH concentrations in agricultural soils ranging from 131.93 to 1699.14 μg·kg^{-1}, with low-molecular-weight PAHs (with 2, 3 aromatic rings) contributing nearly 50% of the total load[4]. These contaminants enter soil systems via atmospheric deposition, wastewater irrigation, and improper waste disposal, accumulating to levels that threaten crop safety, soil biological activity, and human health through trophic transfer[5,6].

Phenanthrene (Phe) is one of the most abundant PAHs (10%–20%) in contaminated agricultural soils[7]. As a three-ring PAH with high lipophilicity and chemical stability, Phe persists in soil for weeks or months, and has a strong tendency to bioaccumulate or phytoaccumulate. Owing to its ubiquity, structural stability, and environmental mobility, Phe is frequently selected as a representative compound for PAH contamination studies[8]. Research on *Brassica parachinensis* (Bok choy) has revealed that low-ring PAHs, such as Phe account for 77.6%–90.3% of the total PAHs assimilated by plants[9]. A similar pattern is seen in Bok choy, which exhibits a bioconcentration factor of 1.5–2.0 for pyrene[10]. With a half-life ranging from weeks to months, Phe can undergo phototransformation into more toxic quinones and impair soil ecological functions by diminishing microbial diversity, suppressing enzyme activities (e.g., urease and dehydrogenase), and disturbing nutrient cycling[11]. Elevated PAH concentrations typically inhibit plant growth. These multifaceted adverse effects underscore the importance of developing efficient remediation approaches for Phe-contaminated soils.

Persulfate (PS)-based advanced oxidation processes (AOPs) have attracted considerable interest because they can rapidly decompose organic pollutants by generating highly reactive oxygen species[12,13]. Because PS requires activation to yield sulfate radicals ($SO_4^{-}\cdot$), which possess superior oxidation potential and longer half-lives than hydroxyl radicals, iron-based catalysts have been widely adopted for this purpose. Materials such as zero-valent iron (ZVI), Fe^{2+} salts, and iron-based nanomaterials are particularly favored due to their low cost, environmental benignity, and high catalytic efficiency[14]. Investigations have demonstrated that under optimized conditions, an Fe^{2+}-thermal coupled activation system achieved a phenanthrene degradation efficiency of 85.1%[15], with sulfate radicals ($SO_4^{-}\cdot$) and hydroxyl radicals (·OH) identified as the primary active species[16]. Likewise, a field-relevant study using natural iron oxides in tropical soil reported 81% Phe removal and 61% mineralization within 24 h under slurry-phase conditions, reaffirming the critical role of $SO_4^{-}\cdot$[17]. These outcomes align with recent advances in plasma-driven AOPs, in which radical-mediated reactions removed 85.52%–99.73% of PAHs[18]. Recent studies have also demonstrated the effectiveness of combined soil washing and AOPs for the remediation of organic-contaminated soils[19–21]. In addition to ZVI and Fe^{2+} salts, other iron-bearing minerals, such as magnetite, hematite, and goethite, have been reported as persulfate activators[22,23].

More recently, Schwertmannite (Sch, $Fe_8O_8(OH)_{8-2x}(SO_4)_x$, where $1.0 \leqslant x \leqslant 1.75$), an iron oxyhydroxysulfate mineral, has emerged as a promising multi-functional catalyst for pollutant degradation. Its distinctive "sea urchin" nanoarchitecture provides a high specific surface area, promoting the adsorption of organic compounds[24]. Compared to conventional iron-based activators such as ZVI and Fe^{2+} salts, Sch has several distinct advantages: (1) it is naturally abundant and can be synthesized from acid mine drainage as a waste-derived material, reducing cost; (2) its high specific surface area and surface-bound Fe^{2+}/Fe^{3+} redox cycle enable sustained PS

activation without external reducing agents; and (3) it exhibits high catalytic activity over a broad pH range (pH 3–9), whereas ZVI and Fe^{2+} salts are often limited by narrow optimal pH and rapid iron precipitation[19,24]. Built-in sulfate groups and a self-sustaining surface Fe^{2+}/Fe^{3+} redox cycle further aid PS activation and catalytic turnover. Sch also performs effectively over a broad pH range (3–9) and can co-stabilize heavy metals, rendering it especially suitable for mixed contamination scenarios commonly encountered in industrial soils[25]. When applied in a Sch/H_2O_2/UV configuration, it achieved 78.8% TOC removal and 90% decolorization from landfill leachates[26]. More recently, Sch activated PS enabled 99.1% degradation of oxytetracycline with 69.7% TOC reduction under UV light, while maintaining high efficiency in complex wastewater matrices[27].

Despite these encouraging results in aqueous environments, using Sch/PS systems for soil remediation (particularly for controlling PAH uptake by crops) has received scant attention. PAHs can translocate from soil into edible plant tissues, posing a direct threat to food safety. As one of the most widely consumed vegetables globally, Bok choy represents a critical pathway for human exposure to PAHs. Therefore, investigating the adsorption of Phe from soil to Bok choy and developing effective interception strategies are of paramount importance for ensuring agricultural products and public health. Unlike previous studies that focused primarily on chemical degradation efficiency in aqueous systems, the present study emphasized the simultaneous assessment of soil remediation performance and crop safety in a soil-plant system. However, the potential of Sch as a persulfate activator for the remediating of PAH-contaminated soil has not yet been determined. To fill this knowledge gap, the present study was conducted with the following specific objectives: (1) determine the Phe degradation efficiency of the Sch-activated PS system in soil; (2) evaluate the ability of the treatment to limit Phe uptake and accumulation in Bok choy and (3) identify the key mechanisms governing Phe degradation and control of its uptake into Bok choy. The outcomes are expected to facilitate the design of sustainable remediation strategies for PAH-affected agricultural soils.

2 Material and methods

2.1 Reagents

Phenanthrene (> 95%, Wako 1st Grade), $FeSO_4·7H_2O$ (> 99.0%), H_2O_2, $Na_2S_2O_8$ (> 97%), acetone (> 99.5%), methanol (> 99.5%), nonane (> 98%), and dichloromethane (> 99.5%) were purchased from Fujifilm Wako Pure Chemical Corporation (Osaka, Japan). Hexane (> 99.5%) was supplied by Wako Pure Chemical Industries, Ltd. (Osaka, Japan). Pyrene-d10 (> 99.99%) was obtained from AccuStandard (New Haven, Connecticut, USA). Silica was provided by Nacalai Tesque, Inc. (Kyoto, Japan). This study used a commercial potting soil specifically formulated for home gardening (Kurotsuchi), purchased from Aichi Engei (Nagoya, Japan). Compound fertilizers were sourced from Aichi Engei (Nagoya, Japan) and Omiya Green Service Company (Saitama, Japan), respectively. Deionized water was prepared using a water purification system (Direct-Q 3 UV, Millipore, Molsheim, USA).

2.2 Preparation of Schwertmannite

The Sch was prepared following the methods of Liu et al.[28]. Briefly, 160 mmol·L^{-1} $FeSO_4·7H_2O$ solution was placed in an Erlenmeyer flask, 1.8 mL H_2O_2 (30%) was added, the flask was sealed with eight layers of gauze, placed in a shaker and incubated at 28 °C and 180 r·min^{-1} for 2 h. Three times, the solid minerals were washed with acid and then deionized water. The minerals were dried at 50 °C, passed through a 100-mesh sieve, and the parameters were analyzed by SEM, XRD, and FTIR, and BET was evaluated.

2.3 Preparation of polluted soil

The organic matter (OM) content in the original soil was 126.02 ± 3.30 g·kg^{-1}. The contents of total nitrogen (TN), total phosphorus (TP) and total potassium (TK) in the original soil were 4.36 ± 0.03, 1.10 ± 0.02, and 5.92 ± 0.00 g·kg^{-1}, respectively. The hydrolyzable nitrogen (HN), available phosphorus (AP) and available potassium (AK) contents in the soil were 471.84 ± 10.27, 2.25 ± 0.10, and 78.7 ± 1.27 mg·kg^{-1}, respectively.

For the experiments, 300 g of soil was collected and placed in a pot measuring 15 cm in depth and 10 cm in diameter. First, acetone-dissolved Phe was added to the soil, with the control having a concentration at 20 mg·kg^{-1}. The resulting mixture was then evaporated in a fume hood. Following a 48-h balance, 1% compound fertilizer, containing 7% total nitrogen, total phosphorus, and total potassium was added to the soil. Subsequently, the soil moisture content was adjusted to 60% of the maximum water-holding capacity.

2.4 Schwertmannite catalyzes persulfate to degradation phenanthrene during the Bok choy growth experiment

Seven treatments were set up (Fig. 1) in seven pots: (1) soil only (black control), (2) soil+Phe, (3) soil+Bok choy, (4) soil+Phe+Bok choy, (5) soil+Phe+Sch+Bok choy, (6) soil+Phe+PS+Bok choy, (7) soil+Phe+Sch+PS+Bok choy. The concentrations of PS and Sch were 200 mg·kg^{-1} and 1 g·kg^{-1}, respectively. Both were applied as a one-time basal application and thoroughly mixed with the soil. After 24 h of equilibration, six seeds were planted in each pot. The pots were then maintained under controlled conditions as these described above, and each treatment was repeated three times. The entire batch of experimental plants was maintained in one shared growth chamber (Biotron NK system, Osaka, Japan), at 24 °C with a 14-h light/10-h dark cycle. Following a 72-h pre-cultivation, five seeds were transplanted into each pot and grown for 50 days under controlled conditions. Their length, fresh weight, and Phe content was then determined.

2.5 Extraction of phenanthrene from soil and Bok choy

The Phe concentrations in plant tissues (leaf, stem, and root) were analyzed using a validated extraction and purification protocol. Homogenized samples (50 mg wet weight) were precisely weighed into 50 mL amber glass vials to minimize photodegradation. Extraction was initiated by adding 20 mL of a dichloromethane/methanol (1:1, v/v) solution and 10 μL of pyrene-d10 internal standard (10 mg·kg^{-1}) for quantification control. The samples underwent three successive 10 min ultrasonic extractions in a temperature-controlled water bath maintained at 25 °C. After each extraction, the supernatant was filtered through a 25-mm glass fiber filter, and the residual solids were re-extraction to ensure maximum analyze recovery. The combined filtrates were processed through a multi-stage concentration and cleanup procedure. Initially, the extract was reduced to 3 mL under reduced pressure (600 torr) at 37 °C using rotary evaporation. A solvent exchange was then conducted by adding 20 mL of hexane/acetone (1:1, v/v) and concentrating the solution again to 3 mL at 180 torr to enhance compatibility with subsequent cleanup steps. The extract was further purified using a silica solid-phase extraction cartridge (500 mg/6 mL) to eliminate interfering pigments and polar compounds. The collected eluate was concentrated to 3 mL under identical pressure conditions (180 torr). Finally, 200 μL of nonane was introduced as a keeper solvent to reduce volatility, and the sample was carefully concentrated under a nitrogen stream to a final volume of 200 μL for instrumental analysis. This method demonstrated high extraction efficiency (> 85%) while maintaining analytical integrity throughout the process.

2.6 Analytical methods

The Phe concentration and purification were performed using a Buchi R-100 rotary evaporation system equipped with I-100 interface and B-100 heating bath (Buchi, Essen, Germany). The evaporation was conducted under reduced pressure (600 torr) with the water bath temperature maintained at 37 °C to prevent thermal degradation of the target compound. The rotation speed was optimized at 120 r·min^{-1} to ensure uniform heating and efficient solvent removal, typically reducing the extract volume from 60 to 3 mL while maintaining high analyte recovery.

Quantitative analysis was carried out on an Agilent 6890A GC-MS system (Agilent, Santa Clara, CA, USA) fitted with an Intertcap 17 capillary column (30 m × 0.25 mm i.d. × 0.25 μm

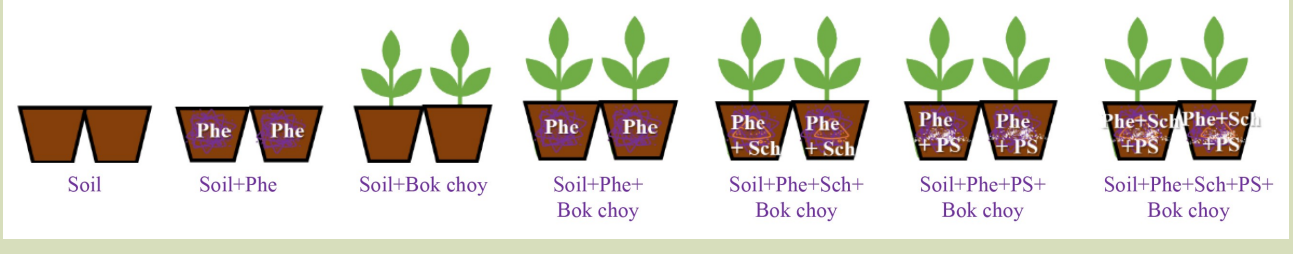


Fig. 1 Treatment design for Schwertmannite-catalyzed persulfate degradation of phenanthrene. Phe, phenanthrene; Sch, Schwertmannite; PS, persulfate.

film thickness). The GC temperature program was set as follows: initial temperature was 40 °C (hold for 2 min) to ensure proper solvent equilibration, increased to 200 °C at 15 °C·min^{-1}, then to 320 °C at 5 °C·min^{-1}, with a final hold time of 8 min to ensure complete elution of high-boiling point compounds. High-purity helium (99.999%) was used as the carrier gas at a constant flow rate of 1.3 mL·min^{-1}. The sample injection volume was 1 μL in splitless mode, with a splitless time of 1.5 min. The injector temperature was maintained at 280 °C to ensure complete vaporization of the analytes.

The MS detection used electron ionization at 70 eV, with the ion source temperature set at 230 °C. The mass scanning range was set at m/z 45–350 to cover the molecular ions and characteristic fragments of the target compounds. The transfer line temperature was maintained at 300 °C to prevent analyte condensation. We compared mass spectra with the NIST 98 library and matching retention times (±0.05 min) with certified standards for compound identification. A five-point calibration curve with correlation coefficients (R^2) exceeding 0.999 was established for quantitative analysis. Data acquisition and processing were controlled using HP Chemstation software, which provided automated peak integration and quantification.

The morphology, mineral phase, and chemical bonds of Sch were characterized using scanning electron microscopy (SEM, S-4800, Hitachi Co., Ltd., Tokyo, Japan), X-ray diffraction (XRD, MiniFlexII, Tokyo, Japan), and Fourier transform infrared spectroscopy (FTIR, IR-6100, JASCO Co., Ltd., Tokyo, Japan), respectively. Soil pH was measured with a Horiba F-73 pH meter (Horiba, Kyoto, Japan) using a 1:2.5 (w/v) soil-to-water ratio after 30 minutes of equilibrium time. Water-soluble ions were analyzed using a Thermo Fisher Scientific ICS-1600 ion chromatography system (Sunnyvale, California, USA) equipped with appropriate anion and cation exchange columns. The system was calibrated using certified reference materials, and quality control samples were analyzed every 10 samples to ensure data reliability. All analyses were performed in triplicate, and method blanks were included to monitor potential contamination.

2.7 Statistical analysis

Microsoft Excel 2019 performed the statistical analysis by calculating the average and standard deviation of triplicate analysis Origin 2021 software plotted the graphs.

3 Results and discussion

3.1 Characterization of Schwertmannite

Figure 2(a) presents the scanning electron microscopy (SEM) image of Sch at 5000× magnification. The material exhibited characteristic aggregation morphology with a rough surface texture featuring numerous acicular protrusions, consistent with the typical Sch structures reported in other studies[29,30].

The X-ray diffraction (XRD) pattern (Fig. 2(b)) showed characteristic diffraction peaks at 2θ = 18.24°, 26.26°, 35.16°, 39.50°, 46.54°, 55.30°, 61.34°, and 63.68°, which matched the standard diffraction pattern for Sch (JCPDS: PDF47-1775) accurately. The specific surface area of the synthesized material was determined to be 18.5 m^2·g^{-1} by BET analysis, which aligned with its aggregated morphology. Additionally, based on an Fe/S molar ratio of 4.66 from elemental analysis (Table 1), the structural formula was established as $Fe_8O_8(OH)_{4.56}(SO_4)_{1.72}$.

The Fourier transform infrared (FTIR) spectrum of Sch is presented in Fig. 2(c). A broad absorption band centered at 3180.34 cm^{-1} corresponded to the O–H stretching vibration of surface hydroxyl groups and structural water. The sulfate vibrational features were clearly identified; a strong, broad band at 1109.08 cm^{-1} was assigned to the ν_3 asymmetric stretching mode of SO_4^{2-}, while the weaker peak at 977.39 cm^{-1} was attributed to the ν_1 symmetric stretching mode. The presence of these two bands indicated sulfate ions forming outer-sphere complexes on the mineral surface. In addition, an absorption peak at 600.44 cm^{-1}, assigned to the ν_4 bending vibration of SO_4^{2-}, suggested sulfates incorporated within the Sch tunnel structure. The peak observed at 690.51 cm^{-1} was characteristic of Fe–O stretching vibrations. All observed absorption features were consistent with those reported in the literature for synthetic Sch[31]. These collective results conclusively demonstrated that the synthesized mineral was Sch.

3.2 The pH during Schwertmannite synthesis

The temporal evolution of pH during Sch synthesis is shown in Fig. 3. The reaction was initiated at pH 3.82. Immediately after adding hydrogen peroxide, the pH decreased sharply to 2.77. This rapid acidification was attributed to the release of protons (H^+) from both the oxidation of Fe^{2+} to Fe^{3+} (Eq. 1)[32] and the

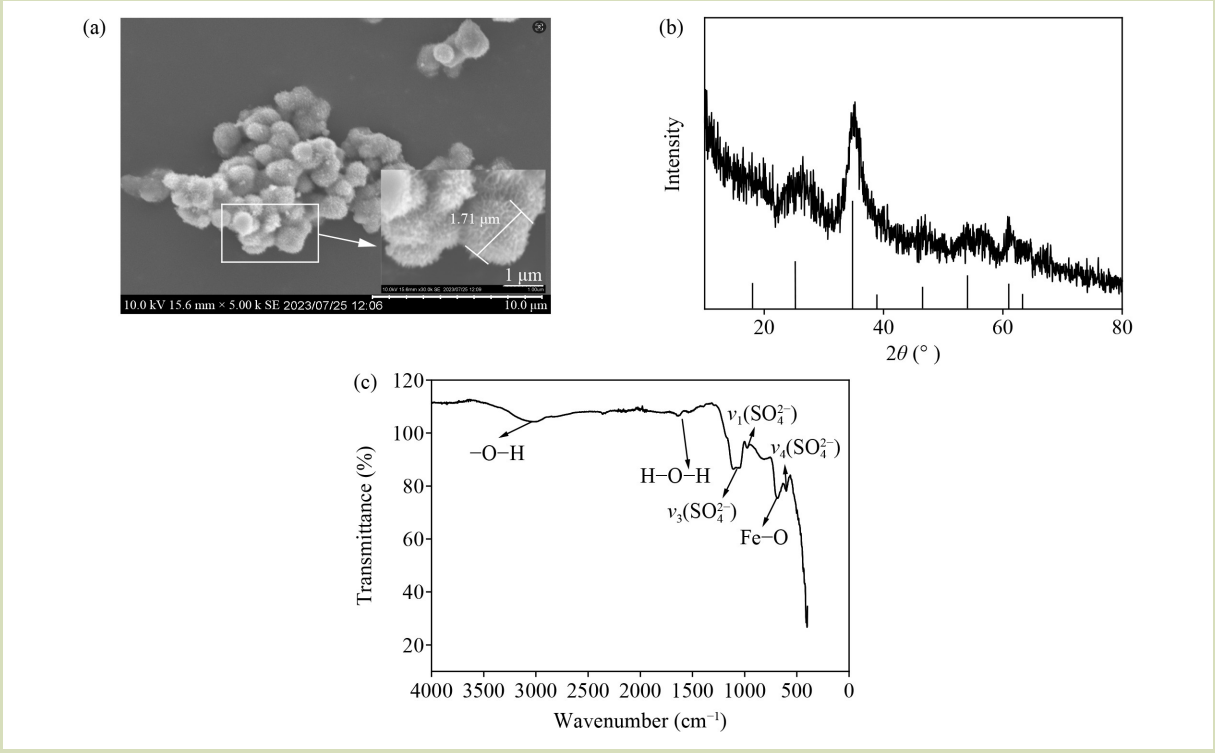


Fig. 2 (a) Scanning electron microscopy (SEM); (b) X-ray diffraction (XRD); (c) Fourier transform infrared spectroscopy (FTIR) of Schwertmannite (Sch).

Table 1 Iron (Fe) and sulphur (S) contents in Sch

Sample	Fe (wt%)	S (wt%)	Fe/S	x	Formula
Sch	54.73	6.717	4.66	1.72	$Fe_8O_8(OH)_{4.56}(SO_4)_{1.72}$

subsequent hydrolysis of Fe^{3+} ions to form species such as $FeOH^{2+}$ (Eq. 2)[33].

$$2Fe^{2+}+H_2O_2+2H^+ \rightarrow 2Fe^{3+}+2H_2O \quad (1)$$

$$Fe^{3+}+H_2O \rightleftharpoons FeOH^{2+}+H^+ \quad (2)$$

Following the initial rapid decrease, the pH continued to decline gradually, reaching 2.34, 2.29, 2.23, and 2.13 at 12, 24, 36, and 48 h, respectively. This progressive acidification reflected the continuous consumption of hydroxyl ions (OH^-) during the nucleation and precipitation of Sch (Eq. 3)[34], which became the dominant process following the initial oxidation and hydrolysis stages. After 60 h, the net proton release ceased, indicating the completion of the precipitation, and the pH stabilized at 2.10.

$$8Fe^{2+} + xSO_4^{2-} + (16-2x)H_2O \rightarrow Fe_8O_8(OH)_{8-2x}(SO_4)_x + (24-2x)H^+ (1 < x < 1.75) \quad (3)$$

3.3 Phenanthrene concentration in the soil during 50 days

Figure 4 illustrates the temporal variation in soil Phe concentration, with Fig. 4(a) specifically showing the evaluation of the effectiveness of different remediation strategies during Bok choy cultivation. After 5 days, the Soil+Phe+Sch+PS+Bok choy system achieved a Phe removal of 86.2%, substantially higher than that of the Soil+Phe+PS+Bok choy (31.9%) and Soil+Phe+Sch+Bok choy (29.8%) systems. In comparison, the Soil+Phe+Bok choy (26.5%) and Soil+Phe

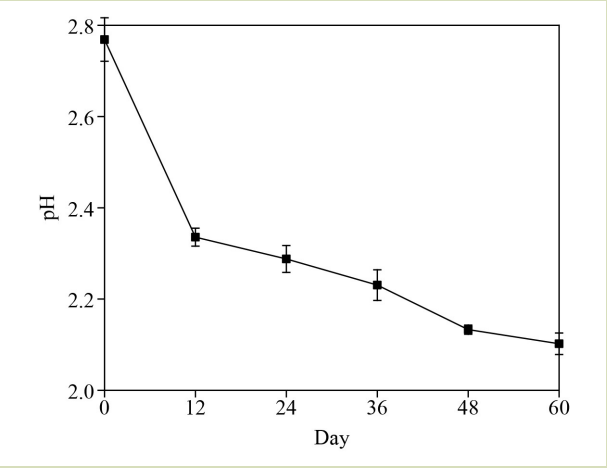


Fig. 3 The pH variation during the synthesis of Schwertmannite (Sch).

(17.6%) treatments showed lower removal efficiencies. By day 10, the Soil+Phe+Sch+PS+Bok choy treatment maintained its superior performance with 84.9% removal. The Soil+Phe+PS+Bok choy treatment showed significant improvement, achieving 61.0% removal, while the Soil+Phe+Sch+Bok choy treatment achieved a moderate 44.8% removal. In contrast, the Soil+Phe+Bok choy system exhibited limited degradation capacity, achieving 41.2% removal, while the Soil+Phe only treatment reached 46.2%. Throughout the 50-day experimental period, all treatments exhibited a progressive increase in Phe degradation efficiency.

By day 30, distinct performance differences were observed among the treatments. The Soil+Phe+Sch+PS+Bok choy system maintained its leading position with 90.1% removal, while the Soil+Phe+PS+Bok choy and Soil+Phe+Sch+Bok choy treatments demonstrated comparable efficiencies of 88.2% and 87.1%, respectively. The Soil+Phe+Bok choy and Soil+Phe treatments showed relatively lower removals of 74.6% and 76.7%, respectively. The Soil+Phe+Sch+PS+Bok choy treatment consistently exhibited the highest performance with 94.5% removal. Notably, the Soil+Phe+Bok choy system showed significant improvement, reaching 89.8% removal, slightly surpassing the Soil+Phe (88.6%).

In comparison, the Soil+Phe+PS+Bok choy and Soil+Phe+Sch+Bok choy treatments achieved final removals of 76.9% and 77.6%, respectively, indicating a stabilization trend in their degradation capabilities during the later experimental phase. In general, all treatments showed an increasing trend in Phe removal efficiency over time. The Soil+Phe+Sch+PS+Bok choy treatment demonstrated excellent capability for Phe removal efficiency, achieving an 86.2% removal within a short period (5 days). This excellent performance was attributed to the large specific surface area of Sch, which provided ample adsorption sites for Phe, as well as weak interfacial interactions (e.g., π–π or cation–π) between the Phe molecules and the mineral surface. Phe removal in the different treatments resulted from distinct physical/biological and chemical oxidation pathways. The Bok choy-containing groups facilitated removal via plant uptake and translocation, whereas the Sch groups relied mainly on adsorption.

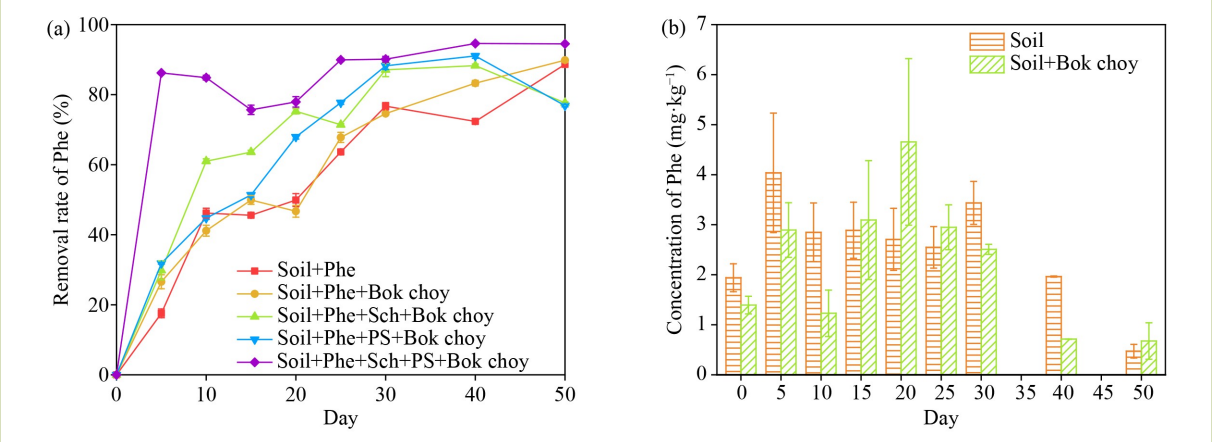


Fig. 4 Dynamics of phenanthrene under different treatments. (a) Schwertmannite (Sch) and/or persulfate (PS) on phenanthrene (Phe)-contaminated soil; (b) blank control (soil only and soil + Bok choy).

In the PS-only treatment, slow activation by native soil iron (Eq. 4) resulted in modest radical-driven oxidation[35]. In contrast, the combined Sch-PS system energized these pathways; Sch adsorbed Phe, while, through its iron-rich surface, efficiently activated PS to produce sulfate radicals ($SO_4^{-}\cdot$) (Eqs. (5) and (6)), thereby enabling rapid and extensive chemical degradation[36]. The decline in Phe concentration in the Soil+Phe treatment group was likely due in part to volatilization, owing to the semi-volatility of the compound, which enabled its diffusion into the atmosphere. As shown in Fig. 4(b), the Phe concentration in the control groups (soil and soil+Bok choy) fluctuated. It was postulated that this observed fluctuation, specifically the initial rise and subsequent fall in concentration, was caused by the migration of volatilized Phe from the adjacent contaminated treatments within the shared enclosure.

$$S_2O_8^{2-} + \equiv Fe^{2+} \rightarrow \equiv Fe^{3+} + SO_4^{2-} + SO_4^{-}\cdot \quad (4)$$

$$SO_4^{-}\cdot + H_2O \rightarrow \cdot OH + H^+ + SO_4^{2-} \quad (5)$$

$$S_2O_8^{2-} + \equiv Fe^{2+} \rightarrow \equiv Fe^{3+} + SO_4^{2-} + SO_4^{-}\cdot \quad (6)$$

3.4 Physiological indicators of Bok choy

Table 2 presents the growth parameters of Bok choy after 50 days of cultivation in phenanthrene-contaminated soil under different remediation treatments. The total plant length (leaf+stem+root) ranged from 19.6 to 32.3 cm in the Soil+Phe+Sch+PS+Bok choy treatment, 13.2 to 37.4 cm in Soil+Phe+PS+Bok choy, 6.1 to 38.3 cm in Soil+Phe+Sch+Bok choy, 16 to 28 cm in Soil+Phe+Bok choy, and 21.6 to 31.6 cm in the Soil+Bok choy control. Notably, the treatments with Sch and PS (Soil+Phe+Sch+PS+Bok choy) showed the narrowest range and a high average plant length, likely because Sch effectively activated PS to generate strongly oxidizing sulfate radicals, which efficiently degraded phenanthrene and thus alleviated its stress on the plants. In contrast, the vastly different plant length ranges in the treatments with PS alone (Soil+Phe+PS+Bok choy), or Sch alone (Soil+Phe+Sch+Bok choy) suggested unstable remediation efficacy, which may have been attributed to insufficient activation of PS and incomplete adsorption/immobilization of phenanthrene, respectively.

Leaf length varied within 8.5–18.2, 9.1–18.4, 10–18.9, 6.9–15.4, and 10.6–15.6 cm across the respective treatments. Stem length measurements showed ranges of 6.4–8.0, 4.6–5.6, 5.6–8.7, 2.1–7.7, and 4.3–7.4 cm, while root length spanned 4.5–11.7, 4.7–15.0, 4.0–12.3, 3.3–7.7, and 6.2–10.3 cm for the five treatments, respectively. Notably, the Soil+Phe+Sch+Bok choy treatment exhibited the maximum observed values in total, leaf, and root length dimensions. This prominent increase in morphological parameters was likely attributed to the effective adsorption and immobilization of phenanthrene by Sch, which reduced the direct phytotoxicity and bioavailability of the contaminant in the soil, thereby allowing for less restricted plant development. Furthermore, the iron-rich nature of Sch may have provided essential micronutrients, potentially stimulating plant growth and contributing to the observed maximum length.

Biomass accumulation in different plant tissues is illustrated in Fig. 5. One-way ANOVA revealed no significant differences among treatments for any biomass parameters ($p > 0.05$). Nevertheless, certain trends were observed. The Soil+Phe+Sch+PS+Bok choy treatment yielded the highest total fresh weight at 6.91 g per pot (Fig. 5(a)), surpassing Soil+Phe+PS+Bok choy (6.63 g per pot) and Soil+Phe+Sch+Bok choy (4.99 g per pot) treatments, which in

Table 2 Leaf, stem, and root lengths of Bok choy under different treatments

Treatment	Total (cm)		Leaf (cm)		Stem (cm)		Root (cm)	
	Max.	Min.	Max.	Min.	Max.	Min.	Max.	Min.
Soil+Phe+Sch+PS+Bok choy	32.3	19.6	18.2	8.5	8	6.4	11.7	4.5
Soil+Phe+PS+Bok choy	37.4	13.2	18.4	9.1	8.8	4.6	15	4.7
Soil+Phe+Sch+Bok choy	38.3	6.1	18.9	10	8.7	5.6	12.3	4
Soil+Phe+Bok choy	28	16	15.4	6.9	7.7	2.1	7.7	3.3
Soil+Bok choy	31.6	21.6	15.6	10.6	7.4	4.3	10.3	6.2

Note: Total, sum of leaf, stem, and root; Phe, phenanthrene; Sch, Schwertmannite; PS, persulfate.

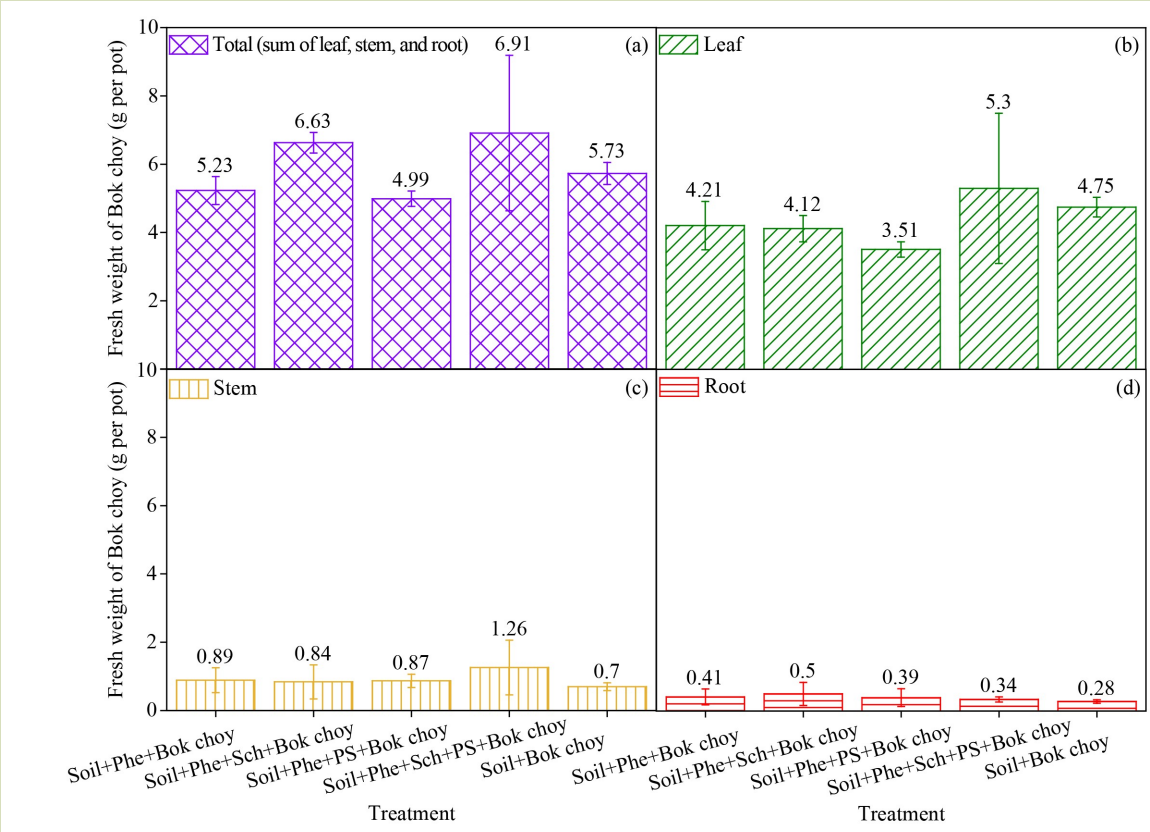


Fig. 5 Fresh weight of *Brassica rapa* subsp. *Chinensis* grown in phenanthrene-contaminated soil under different treatments: (a) total, (b) leaf, (c) stem, and (d) root. No significant differences were found among treatments (p > 0.05). Phe, phenanthrene; Sch, Schwertmannite; PS, persulfate.

turn exceeded the Soil+Phe+Bok choy (5.23 g per pot) and Soil+Bok choy (5.73 g per pot) values. Leaf biomass (Fig. 5(b)) followed the order: Soil+Phe+Sch+PS+Bok choy (5.3 g per pot) > Soil+Bok choy (4.75 g per pot) > Soil+Phe+Bok choy (4.21 g per pot) > Soil+Phe+Sch+Bok choy (4.12 g per pot) > Soil+Phe+PS+Bok choy (3.51 g per pot). Stem weight (Fig. 5(c)) was greatest in Soil+Phe+Sch+PS+Bok choy (1.26 g per pot), followed by Soil+Phe+Bok choy (0.89 g per pot), Soil+Phe+PS+Bok choy (0.87 g per pot), Soil+Phe+Sch+Bok choy (0.84 g per pot), and Soil+Bok choy (0.70 g per pot). Root biomass (Fig. 5(d)) showed a different pattern, with Soil+Phe+Sch+Bok choy recording the highest value (0.50 g per pot), followed by Soil+Phe+Bok choy (0.41 g per pot), Soil+Phe+PS+Bok choy (0.39 g per pot), Soil+Phe+Sch+PS+Bok choy (0.34 g per pot), and Soil+Bok choy (0.28 g per pot). The differences in biomass accumulation primarily originated from the distinct mechanisms of the remediation strategies. In the combined treatment (Soil+Phe+Sch+PS+Bok choy), Sch effectively activated PS to generate sulfate radicals, enabling efficient degradation of Phe and thereby alleviating its inhibitory effect on overall plant growth. In contrast, the Sch-alone treatment (Soil+Phe+Sch+Bok choy) primarily reduced Phe bioavailability in the rhizosphere through adsorption, creating a relatively safer growth environment for roots, which explained its superior performance in root biomass. In summary, the integrated treatment combining Sch and PS demonstrated the most favorable overall growth performance in terms of total biomass production.

3.5 Concentration of Phe in Bok choy

As illustrated in Fig. 6, the concentration of Phe (phenanthrene) in Bok choy varied significantly across treatments. In leaves, the Phe concentrations followed this

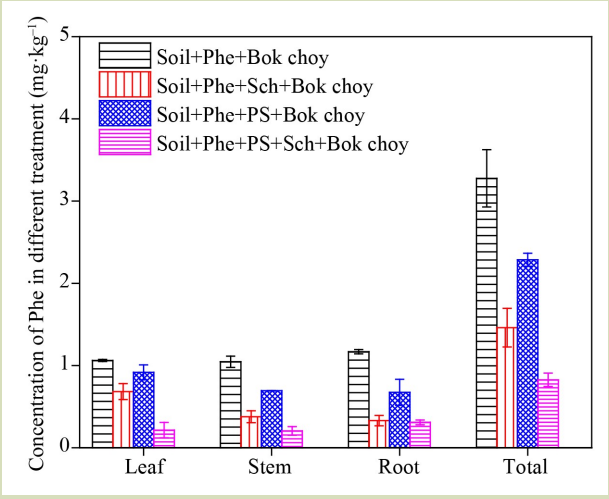


Fig. 6 Migration of Phe in leaf, stem, and root of *Brassica rapa* subsp. *Chinensis*. Phe, phenanthrene; Sch, Schwertmannite; PS, persulfate.

descending order: soil+Phe+Bok choy (1.1 mg·kg^{-1}) > soil+Phe+PS+Bok choy (0.9 mg·kg^{-1}) > soil+Phe+Sch+Bok choy (0.7 mg·kg^{-1}) > soil+Phe+PS+Sch+Bok choy (0.2 mg·kg^{-1}). Similarly, in stems, the trend was: soil+Phe+Bok choy (1.0 mg·kg^{-1}) > soil+Phe+PS+Bok choy (0.7 mg·kg^{-1}) > soil+Phe+Sch+Bok choy (0.4 mg·kg^{-1}) > soil+Phe+PS+Sch+Bok choy (0.2 mg·kg^{-1}). In roots, the order was: soil+Phe+Bok choy (1.2 mg·kg^{-1}) > soil+Phe+PS+Bok choy (0.7 mg·kg^{-1}) > soil+Phe+Sch+Bok choy (0.3 mg·kg^{-1}) > soil+Phe+PS+Sch+Bok choy (0.3 mg·kg^{-1}).

Overall, the lowest Phe accumulation across all plant tissues was consistently observed in the treatment where both PS and Sch were applied together. This remarkable reduction was attributed to a synergistic mechanism between PS and Sch. Specifically, Sch, as an iron-rich mineral, can effectively activate PS to generate powerful sulfate radicals (SO_4^{-}·) and other reactive oxygen species[37,38]. Notably, the surface-bound Fe^{2+}/Fe^{3+} redox cycle on Sch enabled continuous radical generation without added external reducing agents, thereby avoiding the rapid radical quenching commonly observed in homogeneous Fe^{2+} systems[30–32]. Furthermore, the simultaneous presence of Sch and PS initiated an advanced oxidation process in the soil matrix, which enhanced the degradation of the parent Phe compound, and also potentially degraded its intermediate products, leading to a more complete remediation and the lowest observed translocation of Phe into Bok choy plants. This sustained radical production mechanism maintained prolonged oxidative capacity, which was critical for effectively reducing Phe bioavailability in soil throughout the plant growth period.

4 Conclusions

A pot experiment was conducted to investigate the effectiveness of Sch and PS in removing Phe from contaminated soil, and their combined effect on blocking the translocation of Phe from the soil into Bok choy (*B. rapa* subsp. *chinensis*). The study showed that: (1) the combined application of Sch and PS caused rapid degradation of Phe in contaminated soil, achieving a removal of 86.2% within 5 days and reaching 94.5% by the end of the experiment; (2) the co-addition of Sch and PS showed no significant adverse effect on the physiological indices (e.g., length, biomass) of Bok choy ($p > 0.05$); and (3) the combined Sch-PS treatment effectively prevented the uptake and accumulation of Phe from the soil by Bok choy. Therefore, the improvement of Phe-contaminated soil with Sch and PS effectively mitigated the phytoavailability of Phe, thereby reducing its potential transfer into the food chain and its associated health risks to humans. Compared to conventional iron-based activators, this system provided advantages in cost, sustainability, and environmental compatibility. Overall, the Sch-persulfate system represented a promising and environmentally compatible approach for the remediation of PAH-contaminated agricultural soils.

Acknowledgements

This work was supported by JSPSKAKENHI Grant-in-Aid for Scientific Research (B), Japan (JP25K03267) and Grant-in-Aid for Early-CareerScientists, Japan (JP24K20941).

Compliance with ethics guidelines

Yanyan Wang, Weiqian Wang, and Qingyue Wang declare that they have no conflicts of interest or financial conflicts to disclose. This article does not contain any studies with human or animal subjects performed by any of the authors.

REFERENCES

1. Liang C, Yang S S, Xing B L, Li C Q, Yuan F, Wang J J, Dong W Z, Yan S L, Sun Z M. Review and perspective of sulfate radical-based advanced oxidation processes (SR-AOPs) in the remediation of polycyclic aromatic hydrocarbon (PAHs) contaminated soil. *Journal of Environmental Management*, 2025, **390**: 126337
2. Wang J, Tao J G, Wu M C, Sun Y Z, Su Y, Guo X T, Du X Y, Li J, Gan J. Size-dependent vector effects of microplastics on bioaccumulation of hydrophobic organic contaminants in earthworm: a dual-dosing study. *Environment International*, 2024, **186**: 108625
3. Zhang D, Wang J J, Zeng H. Soil polycyclic aromatic hydrocarbons across urban density zones in Shenzhen, China: occurrences, source apportionments, and spatial risk assessment. *Pedosphere*, 2016, **26**(5): 676–686
4. Tao S Y, Zhong B Q, Lin Y, Ma J, Zhou Y Z, Hou H, Zhao L, Sun Z J, Qin X P, Shi H D. Application of a self-organizing map and positive matrix factorization to investigate the spatial distributions and sources of polycyclic aromatic hydrocarbons in soils from Xiangfen County, northern China. *Ecotoxicology and Environmental Safety*, 2017, **141**: 98–106
5. Esmaeili A, Knox O, Juhasz A, Wilson S C. A comparison of *in-vitro* PAH bioaccessibility in historically contaminated soils: implications for risk management. *Soil and Sediment Contamination: An International Journal*, 2021, **30**(8): 901–923
6. Tong X N, Chen X C, Chuang H C, Cao J J, Ho S S H, Lui K H, Ho K F. Characteristics and cytotoxicity of indoor fine particulate matter ($PM_{2.5}$) and $PM_{2.5}$-bound polycyclic aromatic hydrocarbons (PAHs) in Hong Kong. *Air Quality, Atmosphere & Health*, 2019, **12**(12): 1459–1468
7. Dhara A, Dutta R. A review on sources and distribution of polycyclic aromatic hydrocarbons (PAHs) in wetland ecosystem: focusing on plant-biomonitoring and phytoremediation. *Environmental Science and Pollution Research*, 2025, **32**(14): 8743–8765
8. Wilcke W. Global patterns of polycyclic aromatic hydrocarbons (PAHs) in soil. *Geoderma*, 2007, **141**(3-4): 157–166
9. Li X S, Zhou C J, Han E X, Ye Z Y, Liu W J, Xing X L, Qi S H. Linking sedimentary PAH occurrence forms to precision lake pollution management: multidimensional insights *via* three component analysis. *Environmental Research*, 2025, **287**: 123101
10. Sahay S, Inam A, Iqbal S. Risk analysis by bioaccumulation of Cr, Cu, Ni, Pb and Cd from wastewater-irrigated soil to *Brassica* species. *International Journal of Environmental Science and Technology*, 2020, **17**(5): 2889–2906
11. Thavamani P, Malik S, Beer M, Megharaj M, Naidu R. Microbial activity and diversity in long-term mixed contaminated soils with respect to polyaromatic hydrocarbons and heavy metals. *Journal of Environmental Management*, 2012, **99**: 10–17
12. Guo L H, Liu D, Han R Y, Yin A X, Gong G F, Li S, Chen R X, Yang J Y, Liu Z M, Zhi K K. Advances in activation of persulfate by novel carbon-based materials: degradation of emerging contaminants, mechanisms, and perspectives. *Crystals*, 2025, **15**(5): 432
13. Huang W Y, Bianco A, Brigante M, Mailhot G. UVA-UVB activation of hydrogen peroxide and persulfate for advanced oxidation processes: efficiency, mechanism and effect of various water constituents. *Journal of Hazardous Materials*, 2018, **347**: 279–287
14. Zhao Z X, Li Y H, Zhou Y R, Hou Y L, Sun Z Y, Wang W H, Gou J F, Cheng X W. Activation of sulfite by micron-scale iron-carbon composite for metronidazole degradation: theoretical and experimental studies. *Journal of Hazardous Materials*, 2023, **448**: 130873
15. Sun Y C, Zhou J Z, Li D, Liu N, Liu Y Z H, Zhao Y Q. Investigating the degradation mechanism of phenanthrene by Fe^{2+}-activated persulfate. *Environmental Engineering Science*, 2022, **39**(3): 248–258
16. Li H X, Yao Y Z, Zhang J, Du J, Xu S D, Wang C H, Zhang D, Tang J H, Zhao H T, Zhou J. Degradation of phenanthrene by peroxymonosulfate activated with bimetallic metal-organic frameworks: kinetics, mechanisms, and degradation products. *Chemical Engineering Journal*, 2020, **397**: 125401
17. Qutob M, Rafatullah M, Muhammad S A, Siddiqui M R, Alam M. A sustainable method for oxidizing phenanthrene in tropical soil using natural iron as a catalyst in a slurry phase reactor with persulfate assistance. *Environmental Science: Processes & Impacts*, 2024, **26**(8): 1391–1404
18. Wang J S, Wang J, Yang S, Chen X, Chen K W, Zhou G, Liu X, Xu L, Huo S Q, Song P A, Wang H. Multifunctional phosphorus-containing imidazoliums endowing one-component epoxy resins with superior thermal latency, heat resistance, mechanical properties, and fire safety. *Chemical Engineering Journal*, 2024, **485**: 149852
19. Baştürk E, Tulun Ş. Remediation of organophosphate pesticide-contaminated soil using soil washing and advanced oxidation processes. *International Journal of Environmental Science and Technology*, 2024, **21**(6): 5459–5468
20. Handojo L, Ikhsan N A, Mukti R R, Indarto A. Chapter 20-Nanomaterials for remediations of agrochemicals. In: Prasad M N V, ed. Agrochemicals Detection, Treatment and Remediation. Amsterdam: *Elsevier*, 2020, 535–567
21. Borah S N, Koch N, Sen S, Prasad R, Sarma H. Chapter 24-

Novel nanomaterials for nanobioremediation of polyaromatic hydrocarbons. In: Sarma H, Dominguez D C, Lee W Y, eds. *Emerging Contaminants in the Environment*. Amsterdam: *Elsevier*, 2022, 643–667

22. Tian H F, Chen C Z, Zhu T L, Zhu B J, Sun Y F. Characterization and degradation mechanism of bimetallic iron-based/AC activated persulfate for PAHs-contaminated soil remediation. *Chemosphere*, 2021, **267**: 128875
23. Qu S B, Wang R Y, Wei M, Hu X, Song X Y. Advanced oxidation processes mediated by Schwertmannite for the degradation of organic emerging contaminants: mechanism and synergistic approach. *Journal of Water Process Engineering*, 2024, **68**: 106527
24. Wang X Q, Wang Z, Wang T Y, Wang A Q, Wang J P, Zhang Y K, Wang Y B. Electronic structure modulation of Schwertmannite by interfacial chemical bond for enhanced photo-Fenton catalytic activity. *Journal of Catalysis*, 2025, **452**: 116426
25. Wang L, Tsang D C W, Poon C S. Green remediation and recycling of contaminated sediment by waste-incorporated stabilization/solidification. *Chemosphere*, 2015, **122**: 257–264
26. Choi H S, Yang X G, Liu G C, Kim D S, Yang J H, Lee J H, Han S O, Lee J, Kim S W. Development of co-hemin MOF/chitosan composite based biosensor for rapid detection of lactose. *Journal of the Taiwan Institute of Chemical Engineers*, 2020, **113**: 1–7
27. Wang Y Y, Zhou J, Bi W L, Qin J M, Wang G H, Wang Z L, Fu P, Liu F W. Schwertmannite catalyze persulfate to remove oxytetracycline from wastewater under solar light or UV-254. *Journal of Cleaner Production*, 2022, **364**: 132572
28. Liu F W, Zhou J, Zhang S S, Liu L L, Zhou L X, Fan W H. Schwertmannite synthesis through ferrous ion chemical oxidation under different H_2O_2 supply rates and its removal efficiency for arsenic from contaminated groundwater. *PLoS One*, 2015, **10**(9): e0138891
29. Liu F W, Qiao X X, Xing K, Shi J, Zhou L X, Dong Y, Bi W L, Zhang J. Effect of nitrate ions on *Acidithiobacillus ferrooxidans*-mediated bio-oxidation of ferrous ions and pyrite. *Current Microbiology*, 2020, **77**(6): 1070–1080
30. Regenspurg S, Brand A, Peiffer S. Formation and stability of Schwertmannite in acidic mining lakes. *Geochimica et Cosmochimica Acta*, 2004, **68**(6): 1185–1197
31. Boily J F, Gassman P L, Peretyazhko T, Szanyi J, Zachara J M. FTIR spectral components of Schwertmannite. *Environmental Science & Technology*, 2010, **44**(4): 1185–1190
32. Bigham J M, Schwertmann U, Traina S J, Winland R L, Wolf M. Schwertmannite and the chemical modeling of iron in acid sulfate waters. *Geochimica et Cosmochimica Acta*, 1996, **60**(12): 2111–2121
33. Ying H, Feng X H, Zhu M Q, Lanson B, Liu F, Wang X M. Formation and transformation of Schwertmannite through direct Fe^{3+} hydrolysis under various geochemical conditions. *Environmental Science: Nano*, 2020, **7**(8): 2385–2398
34. Dou X M, Mohan D, Pittman C U Jr. Arsenate adsorption on three types of granular Schwertmannite. *Water Research*, 2013, **47**(9): 2938–2948
35. Bi W L, Wu Y L, Dong W B. The degradation of oxytetracycline with low concentration of persulfate sodium motivated by copper sulphate under simulated solar light. *Chemical Engineering Journal*, 2020, **393**: 122782
36. Ji Y F, Ferronato C, Salvador A, Yang X, Chovelon J M. Degradation of ciprofloxacin and sulfamethoxazole by ferrous-activated persulfate: implications for remediation of groundwater contaminated by antibiotics. *Science of the Total Environment*, 2014, **472**: 800–808
37. Wang J L, Wang S Z. Activation of persulfate (PS) and peroxymonosulfate (PMS) and application for the degradation of emerging contaminants. *Chemical Engineering Journal*, 2018, **334**: 1502–1517
38. Xu M J, Zhou H Y, Wu Z L, Li N W, Xiong Z K, Yao G, Lai B. Efficient degradation of sulfamethoxazole by $NiCo_2O_4$ modified expanded graphite activated peroxymonosulfate: characterization, mechanism and degradation intermediates. *Journal of Hazardous Materials*, 2020, **399**: 123103